ADDIS ABABA UNIVERSITY

SCHOOL OF GRADUATE STUDIES

Electrocatalytic Reduction of Oxygen at Poly (4-Amino-3-Hydroxynaphtalene Sulfonic Acid)/Reduced Graphene Oxide Composite

By

Fitsum Addis Hailu

Advisors: Dr. Shimelis Admassie

Dr. Girum Ayalneh

(Master's Thesis)

May, 2017

Addis Ababa, Ethiopia

Electrocatalytic Reduction of Oxygen at Poly (4-Amino-3-Hydroxynaphtalene Sulfonic Acid)/Reduced Graphene Oxide Composite

By

Fitsum Addis Hailu

A thesis

submitted to the department of materials science

in partial fulfillment of the requirements for the degree of

Master of Science

in

Materials Science

Addis Ababa University

Addis Ababa, Ethiopia

May, 2017

ADDIS ABABA UNIVERSITY

School of Graduate Study

Material Science Program

This is to certify that the thesis prepared by Fitsum Addis Hailu, entitled:"*Electrocatalytic Reduction of Oxygen, at Poly (4-Amino-3-Hydroxynaphtalene Sulfonic Acid)/Reduced Graphene Oxide Composite*" and submitted in partial fulfillment of the requirements for the degree of Masters of Science complies with the regulation of the University and meets the accepted standards with respect to originality and quality.

Signed by the examining committee**:**

Dr. Shimelis Admassie Signature _____ Date_____.

Advisor

Dr. Girum Ayalneh Signature _____ Date_____.

Advisor

Dr. Solomon Mehretie Signature _____ Date_____.

Examiner

Dr. Weldegebriel Yohannes Signature_____ Date_____.

Examiner

Acknowledgements

Here I would like to express my sincere gratitude to my advisors, Dr. Shimelis Admassie and Dr. Girum Ayalneh for their visionary guidance, insightful advices and genuine supports in my master's program, without which this thesis would not have been accomplished to its least content. Additionally, I appreciate the great support from PhD students in the laboratory, especially Teklewold Getachew and Fekadu Chekol, who have been always so supportive, helpful and collaborative to the research work demonstrated here. Finally, I would like to thank my parents and sisters for their consistent support of my studies at Addis Ababa University.

Contents

List of Figures

List of Table

List of Abbreviations

HOPG	highly ordered pyrolytic graphite
GO	graphene oxide
CMG	chemically modified graphene
CVD	chemical vapor deposition
GIC	graphite intercalation compounds
rGO	reduced graphene oxide
SSNMR	solid state nuclear magnetic resonance
BSCF	Perovskite ($Ba_{0.5}Sr_{0.5}Co_{0.8}Fe_{0.2}O_{3-\delta}$)
MWCNT	multi wall carbon nanotube
AHNSA	4-Amino-3-hydroxynaphtalene sulfonic acid
RRDE	rotating ring disc electrode
RDE	rotating disk electrode
CV	cyclic voltammetry
RDV	rotating disk voltammetry
DI-Water	deionized water

Abstract

The rapid growth of the global population and industrial activities pose a great challenge to meeting ever-increasing energy demands. This thesis adapts a modified synthesis of graphene oxide (GO), an important starting material in graphene chemistry, convert graphene oxide back to graphene-like structure, and finally shows the electrochemical behavior poly (4-amino-3-hydroxynaphtalene sulfonic acid)/rGO composite and also demonstrates its possible application in electrocatalytic reduction of oxygen. In this work, the electrochemical, XRD, and FTIR analysis gave evidence for the formation of graphene oxide (GO) from graphite and the reduced graphene oxide (rGO) from GO. The electrocatalytic activity of the poly (4-amino-3-hydroxynaphtalene sulfonic acid)/rGO composite modified electrodes towards oxygen reduction reaction were studied. The p-(AHNSA) modified glassy carbon electrode shows a two-electron reduction of oxygen to hydrogen peroxide and the p-(AHNSA)/rGO modified glassy carbon electrode shows a direct four-electron reduction of oxygen to water. Koutecky-Levich plot analysis was used to predict the mechanism and evaluate the kinetic parameters.

1 Introduction

1.1 Electrocatalytic Reduction of Oxygen

Oxygen electrochemistry is the most important issue in the development of fuel cells, metal air batteries, industrial electrocatalytic process and electro-organic reactions [1].

Oxygen reduction reaction (ORR) is sluggish and proceeds through several intermediates which makes challenging for electrochemistry. This requires to search for cheaper materials with excellent electrocatalytic activity towards ORR to replace the commonly used costly metal (Pt) based electrocatalyst and develop new and better electrocatalysts. ORR occurs in various electrochemical energy conversion processes and electrocatalysis of the dioxygen reduction continuous to command a great deal of interest in modern electrochemistry, owing to its technological importance in electrochemical devices. The current research lies in the utilization of modified electrode. The catalytic oxygen reduction reaction is the most important electrochemical reaction in the practical, economical and theoretical point of view [2-4].

The mechanism of oxygen reduction reaction in acidic media involves either the direct 4-electron reduction pathway from O_2 to produce H_2O or the 2-electron reduction pathway from O_2 to form hydrogen peroxide (H_2O_2) [5].

$$O_2 + 4H^+ + 4e^- \longrightarrow 2H_2O \text{ (four-electron pathway)}$$

$$O_2 + 2H^+ + 2e^- \longrightarrow H_2O_2 \text{ (two-electron pathway)}$$

Water is directly produced when oxygen is reduced through the four-electron reduction mechanism. On the other hand, the two-electron reduction occurs at low potentials and produces hydrogen peroxide as an intermediate byproduct.

Now a days, the need for increased energy forced the search for new energy conversion technologies. Hence, electrocatalysis found special place as its concepts present a basis for hydrogen energy, fuel cell technology and to some extent battery technology (considering metal-air batteries) [6]. For electrochemical system, overall rate of conversion of reactants to products at an electrode is measured by a current (I) passing through metal/solution interface. In order to avoid possible discrepancies due to the size of the interface, current is usually normalized by electrode surface area (A), and expressed as current density (j), so reaction rate (v) can be expressed as:

$$\mathrm{v} = \frac{I}{n.F.A} = \frac{j}{n.F} \qquad 1.1$$

where n stands for the number of electrons exchanged in electrochemical reaction and F is Faraday constant (96485 C mol^{-1}). By reordering eq. (1.1), one can immediately draw a conclusion that overall current passing through an electrochemical cell can be increased in two ways: (1) by increasing surface area or (2) by increasing reaction rate.

In the former case the effect is trivial and purely technical. However, the latter case is not, and it is related to electrocatalytic effect. It can be achieved by tailoring chemical, geometric and electronic structure of the surface of an electrode materials. This is true for electrocatalysis which can be defined as dependence of the rate of electrochemical reaction on the nature of electrode materials. In order to avoid any confusion hereafter, quantities in Eq. (1.1) should be defined more precisely. In specific, if one uses geometrical surface area of an electrode to normalize I in terms of current density, such obtained current density should be denoted j_{geom} or

just j. Real surface area of an electrode, or electrochemically active surface areas (ESA), are generally different from geometrical surface area. So, if one of these quantities is used to normalize total current, obtained current density should be denoted as j_{real} or j_{ESA}. It can be concluded that comparison of different electrocatalysts should be based on j_{real} (j_{ESA}) measurement.

Similarly to any chemical system, rate of electrochemical reaction can be changed by temperature, pressure and the concentration of reactants. However, additional control parameter for the rate of electrochemical reaction is the electrode potential (E). However, it's absolute value is not accessible to measurements, so the zero of electrode potential scale is set by introduction of hydrogen scale of electrode potentials for instance. Let us consider an electrode reaction:

$$O + ne^{-} \leftrightarrow R \qquad 1.2$$

If no current is passing through metal/solution interface, the electrode is rested on its equilibrium and the reversible potential (E_r) is given by Nernst equation:

$$E_r = E^o + \frac{RT}{nF} ln \frac{a_o}{a_R} \qquad 1.3$$

Where, E^o is the standard electrode potential of O/R couple. If current is passing through the electrode, electrode potential will be different from E_r, hence, the electrode is polarized. If electrode potential is E for a current density j one can define overvoltage (η) as:

$$\eta = E - E_r \qquad 1.4$$

Truly first equation of electrochemical kinetics, Tafel equation, links overvoltage and current density as:

$$\eta = a + b \,.\log j \qquad 1.5$$

where a and b are certain parameters. For most of the electrochemical reactions parameter b, called Tafel slope, is around 100 mV per decade of current density, so it can be concluded that increase of the overvoltage for approx. 100 mV increases the rate of electrochemical reaction for one order of magnitude. This is what makes the difference between chemical and electrochemical systems: by controlling electrode potential (or overvoltage), the rate of the reaction can be finely controlled or increased tremendously. In addition, based on Eq. (1.5), one can judge the electrocatalytic effect, for a particular electrode reaction, on the basis of the dependence of a and b on the nature of the electrode materials.

Based on Eq. (1.5) one can compare two electrocatalytic materials. For example, if a particular electrode reaction takes place on two different electrode materials with the same current density, more effective electrocatalyst requires lower overvoltage. If overvoltage is the same for both materials, higher current density will be measured at more effective electrocatalyst. Now, let us consider the power (P) necessary for electrode reaction to take place in electrolytic cell, or power gained by some power source. In both cases general expression is:

$$P = U.I \qquad 1.6$$

where U denotes voltage between the anode and cathode, and I denotes current passing through the interfaces (as being serial elements of the equivalent circuit). For example, if one performs electrolysis at constant current, more effective electrocatalytic materials will require lower U, which means that less power will be used. If some power source, working at specific voltage (for example fuel cell), is used, more effective electrocatalytic materials will provide higher current, which means that more power will be gained in this case. No matter which technology is used, if electrode materials catalyze electrode reactions effectively, the costs will be reduced tremendously. Tafel equation is an empirical equation, but development of

the electrode kinetics allowed dipper understanding of charge transfer processes at electrified interfaces. If reaction (1.2) is a single step n-electron charge transfer a general expression holds:

$$i = i_o[e^{-\alpha f\eta} - e^{(1-\alpha)f\eta}] \qquad 1.7$$

f is $\frac{F}{RT}$, α is transfer coefficient. Eq. (1.7) assumes that anodic current is positive and cathodic current is negative and we shall hold to this convention hereafter. Parameter α is related to the kinetics of charge transfer. At high anodic (positive) or cathodic (negative) overvoltage, Eq. (1.7) reduces to the form of Tafel equation, but special care should be taken to correct i for mass transfer limitations, so that only charge transfer effect is accounted for (as mass transfer rate does not depend on electrode material). In that case, Tafel parameter is related to i_o while Tafel slope b is:

$$b = \frac{-\alpha F}{2.3RT} \qquad 1.8$$

For anodic polarization, or

$$b = -\frac{(1-\alpha)F}{2.3RT} \qquad 1.9$$

for cathodic polarization. In the case of complex electrode reaction (which is a general case with electrocatalytic reactions) $i-\eta$ relationship is not as simple, but all the information about electrode process are contained in $i-\eta$ or $i-E$ curve. Hence, acquiring reliable data on $i-E$ relationship is the essential for the estimation of electrocatalytic activity and assessment of kinetic parameters of an electrode reaction. These fundamental data are necessary in order to understand electrocatalytic process and to design new electrocatalytic materials with enhanced properties [7, 8].

1.2 Graphene oxide (GO) and Reduced Graphene Oxide (rGO)

Graphene oxide is a lined two-dimensional carbon sheet with diverse oxygenated functional groups which has a thickness around 1 nm and lateral dimension of few nanometers to several microns. The history of GO was begun by the British chemist B.C. Brodie in 1859. It is a cheapest precursor to produce processable graphene in high quantity and is the most suitable starting material for synthesis of functionalized graphene. The exact structure of GO is difficult to describe precisely due to the complexity of the material, its amorphous, berthollide character (nonstoichiometric atomic composition) and the lack of precise analytical techniques for the characterization of GO [9]. Despite of those difficulties, most of the models proposed so far have described it as a polydispersed material with a structural formula as shown in Figure 1. The intrinsic property of functional groups (i.e., hydroxyl, epoxy, lactol, carbonyl, caboxylic acid and organosulfonate) in GO is highly influenced by the synthesis conditions like reaction time, temperature and procedures of synthesis. Hydroxyl and epoxy groups destroy localized π electrons and results in decreasing carrier mobility and its electrical conductivity which both make it an insulating material (a sheet resistance of about $4x10^{10}$ Ω/sq) [10]. Sheet resistance is the measure of the electrical conductance of the sheet independent of its thickness.

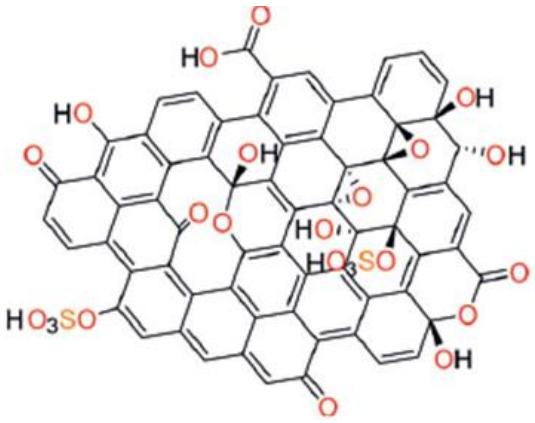

Figure 1. Structural formula of GO with some functional groups (organosulfate, hydroxyl, epoxy, carbonyl, lactol and carboxylic acid) at the edge and both sides of the basal plane [11].

Over oxidation of GO can lead to a release of CO_2 gas, as a consequence defects are formed on the sigma bond of C-skeleton in GO. The main reason of those defects is that the destruction of honeycomb lattice by holes, and additional carbon atoms in five member rings [12]. Despite its difficulty to spot the defects in GO, the defects can be restored and repair holes by heating the GO at higher temperature >1500 ^{0}C [13] which leads to the reduction of GO to reduced graphene oxide.

rGO is one kind of chemically derived graphene and it can be also named as functionalized graphene, chemically modified graphene, chemically converted graphene, or reduced graphene. It is a 2D form of carbon but with chemical moieties that render new functionalities while preserving some properties of pristine material. The chemical exfoliation of graphite through oxidation leads to covalent functionalization followed by reduction which brings reduced graphene oxide. This sequenced process noticeably changes the structure of graphene. Therefore, rGO is not exactly the same as graphene because of the difference in their intrinsic properties [14]. Even though the relativistic intrinsic properties like charge carrier mobility and

conductivity observed in ideal graphene are absent in rGO, flexible processability and versatile properties make rGO interesting in fundamental research as well as application in energy storage. Therefore, due to its ease of processing and unique properties such as mechanical stability, tunable electrical and optical properties, rGO based-thin films provide great hopes for their use in electronic and opto-electronic, wherein components are built on plastic of paper like platforms [15], electrodes [16], ultracapacitors [17], and photovoltaic. The quality of graphene produced depends on the process parameters used when reducing graphene oxide (GO).

1.2.1 Synthesis of Graphene Oxide (GO)

The synthesis of GO is mostly accomplished by wet chemical synthesis methods. There are different methods for the synthesis of GO including Brodie and Staudenmair methods [18], Hummer's method [19] and Tour method [20]. In this section the Hummer's method is only discussed in a little more detailed since it is the most frequently method used for synthesis of GO by delamination a single layer of graphite oxide using proper solvents.

The Staudenmaier, Hummers and Offeman methods are the procedures to prepare GO by using potassium chlorate and fumic nitric acid, or potassium permanganate as oxidant in sulfuric acid solution [9, 11]. However, the products of GO by using those synthesis methods is varied depending on the type of oxidant used, precursors of graphite and reaction conditions. For instance, nitric acid is the common oxidant and known to react strongly with aromatic carbon surfaces and results in the formation of different oxygen containing functional groups such as carboxylic acids, lactones and ketones. During the oxidation process by HNO_3, NO_2 and/or N_2O_4 gases are released as demonstrated by yellow vapor and create a defects in the structure of GO [21, 22]. In addition, potassium chlorate is also another strong oxidizing agent used as reactive species that could affect the properties of final product accordingly. Jones' reagent

(H_2CrO_4/H_2SO_4) is also a commonly used oxidant for the formation of expanded graphite during the synthesis of GO. In the Hummers method the mixture of potassium permanganate and sulfuric is mostly applied as an oxidant. In this procedure, despite permanganate is a known oxidizing agent (i.e. dihydroxilations), as a matter of fact dimanagneseheptoxide is more reactive species than the potassium permanganate counterpart. The formation of dimanganeseheptoxide from $KMnO_4$ is shown in the following scheme [23].

$$KMnO_4 + 3H_2SO_4 \rightarrow K^+ + MnO_3^+ + H_3O^+ + 3HSO_4^-$$

$$MnO_3^+ + MnO_4^- \rightarrow Mn_2O_7$$

In general, the flow chart of modified Hummer's method for the preparation of GO is depicted in Figure 2.

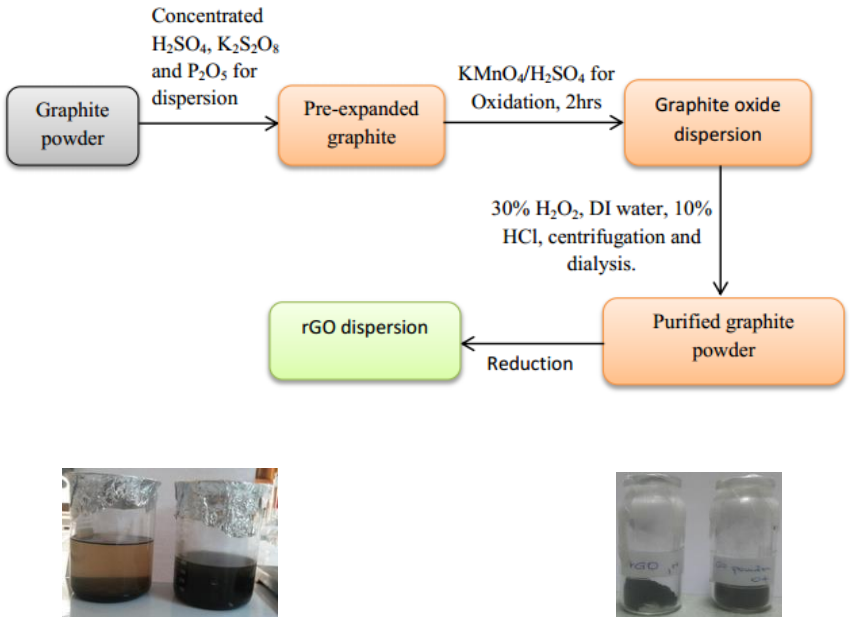

Figure 2. Schematic of modified Hummers method for GO preparation [10].

1.2.2 Synthesis of Reduced Graphene Oxide (rGO)

rGO can be synthesized either from graphite or GO as a starting materials by using various methods such as chemical, thermal, and electrochemical reduction methods. GO is the most convenient starting material for the synthesis of rGO since the degree of exfoliation achieved by graphite is lower than that of GO as supported by the presence of graphitic diffraction peak in the XRD patterns [24].

Chemical reduction method is the most widely used procedure and involves reducing of GO by different strong reducing agents such as hydrazine [25], dimethylhydrazine [26], hydrides (lithium, potassium or sodium hydrides), and hydroquinone [26]. The main objective of any reducing procedure is to synthesize graphene like material achieved directly from mechanical exfoliation. One of the main disadvantages in chemical reduction method, specially using hydrazine, is the introduction of impurities due to the presence of hetroatoms like oxygen and nitrogen in the rGO network. Removing nitrogen functionalities which are bonded covalently on the surface of GO is more difficult than oxygen functionalities. Then the electronic properties of the resulted material greatly affected by C-N groups which are functioning as n-type dopant [27, 28].

Thermal reduction is achieved by the direct heating of GO at elevated temperature about 1050 ^{0}C in the furnace. Nevertheless, the main disadvantage of thermal exfoliation is the structural destruction due to the release of CO_2 which causes the loss of GO about 30 % and create vacancies and defects though out the plane of rGO. Those defects adversely affect the electronic property of the product by decreasing the ballistic transport path length [29].

Electrochemical technique involves the electrochemical removal of oxygen functionalities from GO and produces rGO. This procedure is advantageous over chemical reduction of GO because electrochemical reduction method doesn't involve strong reducing agent chemicals (e.g., hydrazine compounds), hence environmental friendly as there are no unnecessary byproducts during and at the end of synthesis. However, the reduction method is still not clear and yet to be discovered in more detail. But, some of the authors proposed that the hydrogen ions have significant role in the reaction path way as shown in the following scheme [30].

$$GO + aH^{+} + be^{-} \rightarrow rGO + cH_2O$$

Since rGO is deposited onto the surface of electrodes during electrochemical reduction of GO in a buffer solution, the method itself has not been demonstrated on a large scale sample. Scaling up the production is the most basic requirement of a synthetic procedure if graphene is meant to be utilized largely. GO film can be coated onto different insulating or conducting substrates surface such as flexible plastic, glass, indium tin oxide (ITO), glassy carbon (GC) and gold (Au). The deposition can be accomplished by using different techniques such as drop-casting [31], deep coating, spraying [32], spin coating [33] and electrophoresis [34]. After deposition of GO film onto the substrate, electrodes can be placed at the opposite end of the film and linear sweep voltammetry can be applied in sodium buffer solution [9, 34]. Moreover, rGO/graphene can be synthesized using fast electrochemical exfoliation of graphite technique in sulfuric acid solution [34]. In a typical procedure, graphite was used as electrode and exfoliated into thin graphene, mainly AB- stacked bilayered graphene with large lateral size. The produced graphene sheets were dissolved in DMF and they can self-aggregate at air-DMF interface. Interestingly, the film obtained exhibits a sheet resistance of <1 kΩ/sq after nitric acid treatment [35].

1.3 Objectives

1.3.1 General objective

The general objective of this study is to synthesize GO, rGO and examine the significance of electrocatalytic reduction of oxygen at poly (4-amino-3-hydroxynaphtalene sulfonic acid)/reduced graphene oxide composite modified glassy carbon electrodes.

1.3.2 Specific objectives

The specific objectives of the study are

1. To modify a conventional glassy carbon electrode with graphene oxide, p-(AHNSA)/rGO nano-composite.
2. To investigate the electrochemical behavior of GO, rGO and p-(AHNSA)/rGO nano-composite.
3. To study the behaviors of GO, rGO and graphite with X-ray diffraction patterns.
4. To compare the performances of the produced GO, rGO and graphene/polymer nanocomposites with reports in the literature.

2 Review of Electrochemical and Spectroscopic Methods

2.1 Electrochemical methods

2.1.1 Linear sweep & Cyclic voltammetry

Voltammetry is an analytical technique relies on the measure of the current flowing through an electrode, the working electrode, dipped in a solution containing electro-active compounds, while a potential scanning is imposed upon it. The working electrode could be made with several materials such as gold, platinum, glassy carbon or any carbon based material. However, if it is made of a drop of mercury rhythmically dropping from a capillary, the analytical technique is called polarography. Mostly, it has a very little surface in order to assume quickly and accurately the potential imposed by the electrical circuit [36].

Voltammetry is a versatile technique for research purposes, it allow to search into several aspects of the electrochemical reactions, namely those reactions in which electrons exchanges are involved between reactants and products. For such reactions, it is possible to investigate on the laws governing the dependence of the current by the potential imposed on an electrode dipped into the reaction environment. Generally, those laws are very complicated, like the redox reactions and the environment in which they are taking place. Hence, voltammetric techniques are the basis of the comprehension of the laws concerning several electrochemical phenomena and have a great importance in several technological fields [37].

Among several voltammetric techniques, the Linear Sweep Voltammetry (or Rapid Scan Voltammetry) is the simplest system. In this technique, the working electrode is supplied with a rapid potential scanning that varies linearly. The scanning starts before the discharging potential and stops afterwards. The capacitive current increases when the velocity of scanning is increased

and cannot be electronically compensated. Hence, the performance, of this technique is strongly restricted.

In linear sweep voltammetry (LSV), the current passing through the working electrode is measured, while the potential between the working electrode and the reference electrode is swept linearly in time, between two preset values. The characteristics of the linear sweep voltammogram depend on a number of factors including (i) the rate of the electron transfer reaction (s), (ii) the chemical reactivity of the electro active species and (iii) the potential sweep rate.

In LSV measurements, the current response is plotted as a function of voltage rather than time. The scan begins from preset potential E_1 where negligible current flows. In general case, as the voltage is swept further to more reductive values a current begins to flow and goes through a maximum before dropping (Figure 3).

To explain this occurrence we need to consider the influence of voltage on the equilibrium established at the electrode surface. The exact form of the voltammogram can be deduced by considering the voltage and mass transport effects. Let us consider that at the electrode surface equilibrium is established, identical to that predicted by the Nernst equation (Equation 1.3). As the voltage is initially swept from E_1 the equilibrium at the surface begins to alter and the current starts to flow. The current rises as the voltage is swept further from its initial value as the equilibrium position is shifted due to the decrease of the concentration of the reactants and increase of the concentration of the products in the vicinity of the electrode surface. The peak occurs, since at some point the diffusion layer has grown sufficiently above the electrode so that the flux of reactant to the electrode is not fast enough to satisfy that

required by the Nernst equation. At this point the current begins to drop. The current decay follows the same behavior as that predicted by the Cottrell equation [7].

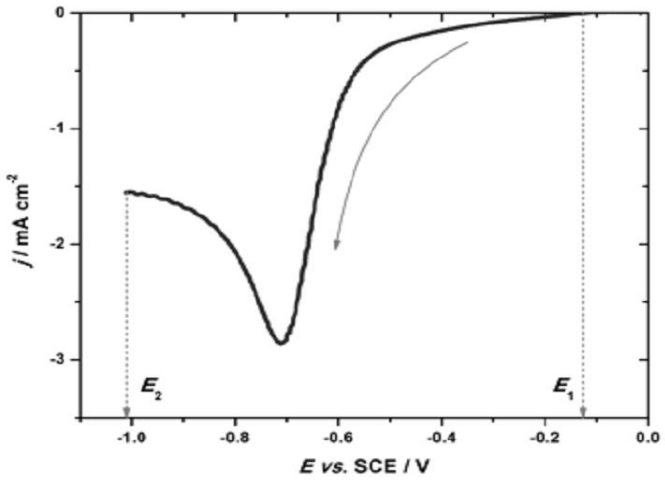

Figure 3. General form of linear sweep voltammogram. In this specific case, electrocatalytic hydrogen evolution from mild acidic solution on tungsten electrode is considered; potential sweep rate was 50 mV s^{-1} [7].

If a series of linear sweep voltammograms is recorded at different scan rates one may observe that the measured current increases with raising scan rate. This can be explained by considering the size of the diffusion layer and the time taken to record the scan. Clearly the linear sweep voltammogram will take longer to record as the scan rate is decreased. Therefore the size of the diffusion layer above the electrode surface will be different depending upon the potential sweep rate used. In a slow voltage scan the diffusion layer will grow much further from the electrode in comparison to a fast scan. Consequently, the flux to the electrode surface is considerably smaller at slow scan rates than it is at faster rates. As the current is proportional to the flux towards the electrode, the magnitude of the current will be lower at slow potential sweep rates and higher at high rates. Actually, is potential is swept slow enough, concentration gradients will

also be at its lowest values, that is stationary ones, and such kind of potential sweep is called quasi-stationary. What is "slow enough" depends actually on mass transfer rate and charge transfer kinetics of a given reaction. This highlight an important point when examining LSV (and cyclic voltammetry, see further on): although there is no time axis on the graph, the voltage scan rate does strongly affect the behavior seen [37].

For an electrode reactions which have rapid electron transfer kinetics it is characteristic that the position of the current maximum occurs at the same voltage. These rapid processes are often referred to as reversible electron transfer reactions. For electron transfer processes that are slow, relative to the voltage scan rate, it is characteristic that the position of the current maximum shifts. In this case the applied voltage will not result in the generation of the concentrations at the electrode surface predicted by the Nernst equation. This happens because the kinetics of the reaction are 'slow' and thus the equilibria are not established rapidly. In this situation the overall form of the voltammogram recorded is similar to that of reversible electron transfer reactions, but now the position of the current maximum shifts depending upon the reduction rate constant and the voltage scan rate. This occurs because the current takes more time to respond to the applied voltage than in the reversible case. For these cases the reactions are referred to as quasi-reversible or irreversible electron transfer reactions [37].

Cyclic voltammetry (CV) is a technique applies to the theoretical study of the behavior of redox couples. Cyclic voltammetry is a particular LSV that perform a triangular shaped scanning at the working electrode. Therefore, the redox couple in solution is exposed before an oxidation and afterwards to a reduction or vice versa.

Cyclic voltammetry (CV) is very similar to LSV. In this case the potential is swept between two values at a fixed rate. However, when the potential reaches E_2 the scan is reversed and the voltage is swept back to E_1 (Figure 3). The forward sweep produces an identical response to that seen for the LSV experiment, but backward response depends on charge transfer kinetics [37].

For a reversible electrochemical reaction the CV recorded has certain well defined characteristics. These are

- The voltage separation between the current peaks is given as:

$$/E_p - E_{1/2}/= \frac{28.5}{n} mV \qquad 2.1$$

- The peak currents are proportional to the square root of the scan rate and is given as:

$$j_p = 2.69x10^{-5} n^{\frac{1}{2}} D^{\frac{1}{2}} \mathrm{v}^{\frac{1}{2}} C \qquad 2.2$$

- The positions of peak voltage do not alter as a function of voltage scan rate
- The ratio of the peak currents is equal to one.

The CV for cases where the electron transfer is not reversible shows considerably different behavior from their reversible counterparts. For quasi-reversible or irreversible electrochemical reaction the recorded CV has following characteristics [37].

- The voltage separation between the current peaks differs from that given in equation 2.1.
- The peak currents are a function of the applied potential.
- The positions of peak potential are a linear function of the logarithm of sweep rate.

By analyzing the variation of peak position as a function of a scan rate, it is possible to gain an estimate for the electron transfer rate constants. Adsorption processes on electrode surface can be distinguished from charge transfer processes, as in former case cyclic voltammogram is symmetrical around potential axes.

2.1.2 Rotating Disk Voltammetry (RDV)

Mass transport of the reactant to a static electrode in a quiescent solution is diffusion limited. Mass transport can be increased by using a rotating disc electrode (RDE), an electrode attached to an electric motor that has a fine control over the electrode‘s rotation rate.

As the disk turns, some of the electrolyte solution is dragged by the disk surface and pushed away from the electrode center by centrifugal forces. The solution is replenished by a laminar flow from the bulk, perpendicular to the disk surface. The flow rate can be controlled by varying the rotation angular velocity of the RDE. The steady state current is now controlled by the laminar flow of the solution in addition to the diffusion. The diffusion term remains because there is stagnant layer at the electrode surface (that rotates with the disk) in which mass transfer is diffusion limited. The thickness of the diffusion layer (δ) is given as:

$$\delta = 1.61 D^{\frac{1}{3}} \nu^{\frac{1}{6}} \omega^{\frac{1}{2}} \qquad 2.3$$

where D, ν and ω stand for diffusion coefficient, kinematic viscosity and disk rotation rate, respectively.

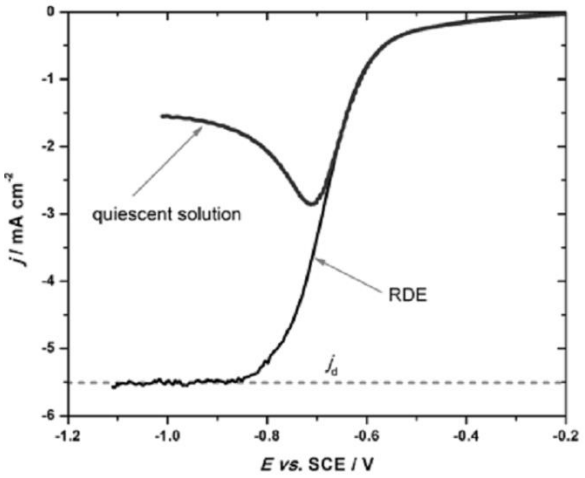

Figure 4. LSV curve from recorded in quiescent solution and LSV of the same electrochemical reaction using rotating disk electrode (RDE) [7].

The higher the rotation speed of the disk, the thinner this layer and therefore the higher the diffusion rate. Once the equilibrium at the electrode surface is reached a current plateau is observed, and the concentration of the reactant at the disc surface is zero. By measuring LSV or CV curves at different RDE rotation rates, various electrochemical phenomena can be investigated. One that is particularly interesting to electrocatalytic reduction of oxygen is the apparent number of electrons transferred.

Levich showed the following relationship between the diffusion controlled current, sometimes called Levich current j_d, and the disk rotation rate (ω):

$$j_d = 0.62nFD^{\frac{2}{3}}\nu^{-\frac{1}{6}}\omega^{\frac{1}{2}}C \qquad 2.4$$

A linear plot of j_d vs. $\omega^{\frac{1}{2}}$, the Levich plot, implies that the electrocatalytic reaction is faster than the rate of substrate delivery to the electrode, so the current is limited only by mass transport to

the catalyst surface. Also, it allows the determination of diffusion coefficient from the slope if other variables are kept constant.

For a reaction mediated by a catalyst surface, a kinetic term must be taken into account. Kinetic current (j_k) represents the current in the absence of any mass-transfer effects, that is, the current that would flow under the kinetic limitation if the mass transfer were efficient enough to keep the concentration at the electrode surface equal to the bulk value, regardless of the electrode reaction. The kinetic current is given by:

$$j_k = nFkC \qquad 2.5$$

Koutecky-Levich expression, which describes the overall current density measured at RDE, for an electrocatalytic reaction over the entire potential range:

$$\frac{1}{j} = \frac{1}{j_k} + \frac{1}{j_d} = \frac{1}{j_k} + \frac{1}{B\omega^{\frac{1}{2}}} \quad , \qquad 2.6$$

($j_d = 0.20nFCD^{\frac{2}{3}}\nu^{-\frac{1}{6}}\omega^{\frac{1}{2}} = nB\omega^{\frac{1}{2}}$)

B is the Levich constant, n is the number of electrons transferred in the reaction, F is the Faraday constant D is the diffusion coefficient ($2.1\text{x}10^{-5}$ cm^2 s^{-1}) in 0.5 M H_2SO_4, ν is the kinematic viscosity ($1.075\text{x}10^{-2}$ cm^2 s^{-1}), C is the concentration of oxygen in the solution (1.1 mM), and ω is the electrode rotational speed (rpm) [38].

A plot of j^{-1} against $\omega^{-\frac{1}{2}}$ should yield a straight line whose slope is related to the number of electrons transferred in the reaction, and whose intercept is related to the kinetic current.

This can be used in order to determine the kinetically limited current density of catalyst materials at various potentials (eliminating the effects of diffusion) and if desired, the number of electrons transferred which will provide indication of the mechanism of any given process.

From the Kouteckye-Levich plot the intercept at the origin $\omega \to \infty$ gives the inverse of the kinetic current density j_k. The dependence of the kinetic current density on the overpotential may be expressed as:

$$\frac{1}{j_k} = \frac{1}{j_l} + \frac{1}{j_o} exp(\frac{/\eta/}{b}) \qquad 2.7$$

The Tafel slope and exchange current density can be calculated using the relation:

$$\eta = E - E_{eq} = -b\{ln\frac{j_l}{j_o} + ln[\frac{j_k}{j_l - j_k}]\} \qquad 2.8$$

Plotting η or E vs. $\ln[\frac{j_k}{j_l - j_k}]$ gives $-b$ as a Tafel slope and the intercept at the origin was used to calculate j_o (exchange current density) using the known limiting current density [38].

When working with RDE, thickness of the diffusion layer is determined by the rotational angular velocity (Equation (2.3)). For every given rotation rate there is an upper limit in sweep rate for which maxima, characteristic for voltammetry in quiescent solution, are not present. For example, in aqueous solutions at room temperature, for angular velocity of 5 rps (revolutions per second) shape of the $j-E$ curve remains unchanged up to sweep rates of 50 mV s^{-1}. Conversely, for angular velocity of 2 rps, sweep rate of 50 mV s^{-1} is too excessive, and characteristic current maxima in voltammetric curve can occur [7].

2.2 Spectroscopic Methods

2.2.1 X-ray Diffraction

X-rays were discovered by Wilhelm Rontgen, a German scientist in 1895. To generate x-rays at least the following three things are required: a source of electrons, a means of accelerating the electrons at high speeds and a target material to receive the impact of the electrons and interact with them.

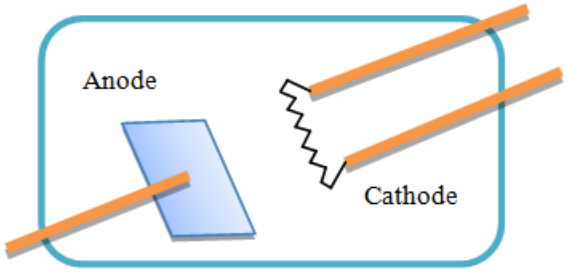

Figure 5. A schematic of X-ray tube.

A typical cathode element is Tungsten (W) with potential of 20-50 KV and the anodic material should be water cooled. The frequency (wavelength) depends on the anode material, usually Cu, Mo, or Co.

Lines occur because bombarding electrons knock out e^- from K shell ($n = 1$), which are filled by electrons in higher shells. Electrons falling from L shell ($n = 2$) give rise to K_a lines, whereas e^- from M shell ($n = 3$) give the K_b lines. ($K_{\alpha 1}$ and $K_{\alpha 2}$ doublets, etc.) [39].

Monochromatic radiation or a narrow range of wavelengths is required for X-ray diffraction. Typically, the K_α line is selected and the K_β line is filtered out by using a thin metal foil of the adjacent $(Z - 1)$ element, for example Nickel filters K_β line of copper. A monochromatic beam

of X-rays can also be selected by reflecting from a plane of a single crystal. The observed intensity I is given by: $I = I_o e^{-\mu t}$. Where, μ is a linear absorption coefficient and t is the path length through which the X- rays are moving [39].

Max Von Laue used a crystal of copper sulfate as the diffraction grating (Nobel Prize 1914).

Crystalline solids consist of regular arrays of atoms, ion, or molecules with interatomic spacing on the order of 100 pm or 1 Å.

The wavelength of the incident light has to be on the same order as the spacing of the atoms.

W.H. and W.L. Bragg determined crystal structures of NaCl, KCl, ZnS, CaF_2, $CaCO_3$, C (diamond). Reflection of X-rays only occurs when the conditions for constructive interference are fulfilled [39].

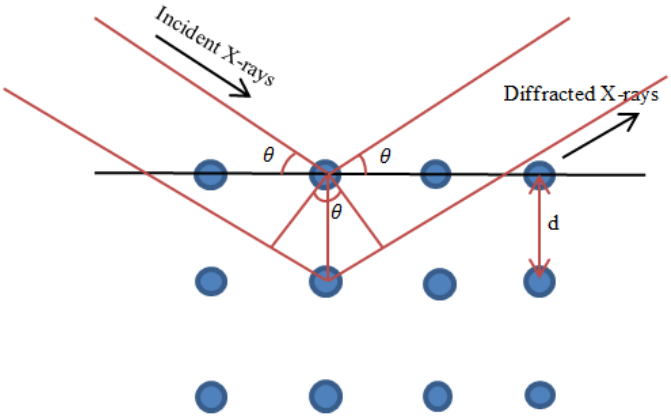

Figure 6. Representation of X-ray travel in crystal lattice.

W.H. and W.L. Bragg showed that the difference in path length, i.e. ($2d_{hkl}sin\theta_{hkl}$) must be an integral number of wavelengths. And this relation is known as Bragg's equation [40].

$$n\lambda = 2d_{hkl}sin\theta, \quad (n = 1,2,3, \dots .) \qquad 2.9$$

2.2.2 Fourier transform infra-red spectroscopy (FTIR)

FTIR is the preferred method of infrared spectroscopy. In infra-red spectroscopy, IR radiation is passed through a sample. Some of the infrared radiation is absorbed by the sample and some passed through or transmitted. The resulting spectrum represents the molecular absorption and transmission, creating a molecular fingerprint of the sample. Like a fingerprint no two unique molecular structures produce the same infrared spectrum. This makes infrared spectroscopy useful for several types of analysis. Therefore, from FTIR we may obtain both qualitative and quantitative material's information [41, 42].

During the sample analysis process, the infrared energy is emitted from a glowing black-body source. This beam passes through an aperture which controls the amount of energy presented to the sample and ultimately to the detector. Then, the beam enters the interferometer where the spectral encoding takes place. The resulting interferogram signal then exits the interferometer. The beam enters the sample compartment where it is transmitted through or reflected off the surface of the sample, depending on the type of analysis being accomplished. This is where specific frequencies of energy which are uniquely characteristic of the sample are absorbed. Finally, the beam passes to the detector for final measurement. The detectors are specially designed to measure the interferogram signal [41].

Then, the measured signal is digitized and sent to the computer where the Fourier transformation takes place. The final infrared spectrum is now presented to the user for interpretation and any further manipulation.

In FTIR there needs to be a relative scale for the absorption intensity, hence a background spectrum must also be measured [41].

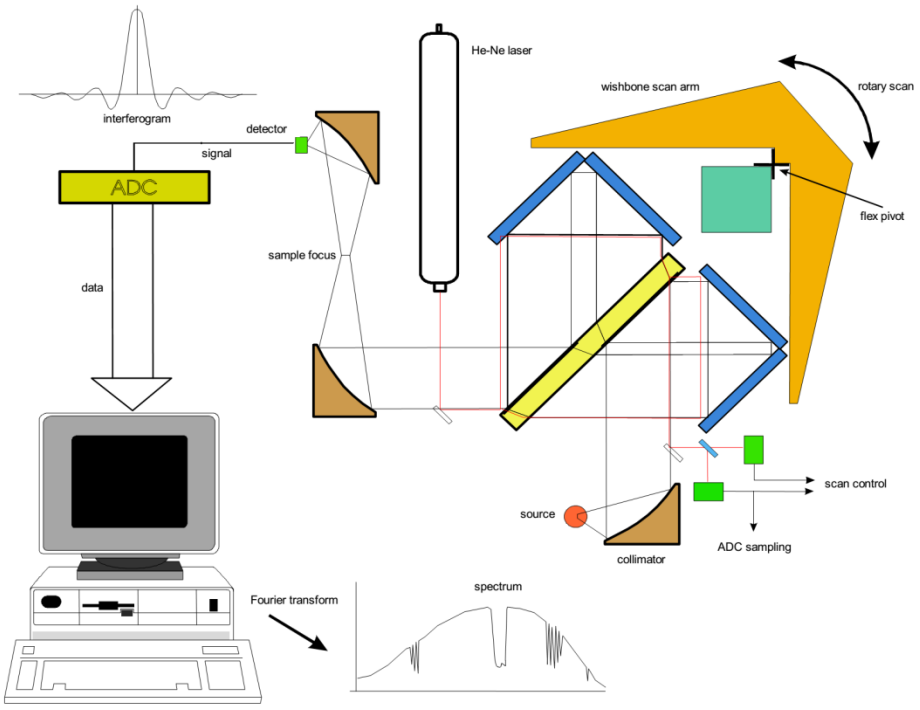

Figure 7. Representation of FTIR spectrometer.

3 Experimental

3.1 Chemicals

The chemicals used in this work include: graphite, $NaNO_3$, KCl, Nafion and Ascorbic acid (Sigma Aldrich); H_2SO_4, H_2O_2 (30%), and HCl (Carlo Erba); $KMnO_4$, $K_3[Fe(CN)_6]$ and 4-Amino-3-hydroxynaphtalene sulfonic acid (BDH Chemicals Ltd.).

3.2 Equipment

Electrochemical measurements were carried out using Metrom Autolab (PGSTAT 128N), with a conventional three electrode systems. Ag/AgCl/KCl (3.0 M), platinum wire and modified glassy carbon electrode were used as reference, counter and working electrode, respectively. Infrared spectra and X-ray diffraction patterns of GO and rGO were collected using a Fourier transform infrared (FTIR) spectrometer (model: PerkinElmer spectrum 65) and XRD instrument with Cu-K (α) radiation at wavelength, λ = 0.154 nm (model: Miniflex 600). Vacuum oven (Model: OV-11/12) was used for drying and boiling purposes. For dispersion and uniform solution formation sonicator (model: Branson 2510) was used.

Figure 8. Equipment used (upper left Metrohm Autolab PGSTAT and right Digital Balance, middle left Sonicator and right X-ray equipment, lower left Vacuum Oven and right FTIR Spectrometer.

3.3 Synthesis of Materials

3.3.1 Graphene oxide (GO) Synthesis

Graphene oxide (GO) was synthesized from graphite powder using modified Hummer's method. In brief, 1 g of graphite and 0.5 g of sodium nitrate were mixed together followed by the addition of 23 ml of concentrated sulphuric acid under constant stirring. After one hour, 3 g of $KMnO_4$ was added gradually to the mixture while keeping the temperature less than 20^oC to prevent overheating and explosion. The mixture was stirred at 35^oC for 6 hrs and the resulting solution was diluted by adding 500 ml of water under vigorous stirring. To ensure the completion of reaction with $KMnO_4$, the suspension was further treated with 30 % H_2O_2 solution (5 ml). The resulting mixture was washed with HCl and H_2O, followed by filtration using filter paper (ASTME 832-81). After filtration, the synthesized GO was dried in vacuum oven and resulted in graphene oxide.

3.3.2 Chemical Reduction of Graphene Oxide (rGO)

The as-prepared graphene oxide suspension was dispersed in deionized water (2 mg ml^{-1}) and sonicated to obtain a homogeneous GO dispersion. The dispersed GO was chemically reduced by sequentially adding 6 mg of ascorbic acid. Successively, the dispersion was kept at 90^oC for 3 hr to produce the reduced graphene oxide (rGO).

3.3.3 Electrochemical Reduction of Graphene oxide

The electrochemical reduction of the as-prepared GO suspension was performed as follows: 12 µl of the graphene oxide dispersion (0.5 mg ml^{-1}) was drop-casted onto the pre-polished glassy carbon electrode, and was left to dry slowly in ambient conditions. Upon drying, 6 µl of 0.05 wt. % Nafion solution was then applied to the surface of the resulting electrode, which was allowed to dry again in ambient conditions [43]. Then the resulting electrode was labeled as the

GO electrode. After this, reduction was performed electrochemically with potential ranging from -1.5 V to 0 V with respect to Ag/AgCl reference electrode in a standard three-electrode electrochemical cell containing 1 M KOH electrolyte, at a scan rate of 50 mV s^{-1} for 10 segments.

3.3.4 Fabrication of p-(AHNSA)/rGO/Glassy Carbon Rotated Disk Electrode (GCRDE)

Electrosynthesis of p-(AHNSA) at GCRDE were carried out from a monomer solution of 2 mM AHNSA in 0.1 M HNO_3 using cyclic voltammetry by scanning the potential between – 0.8 V and +2.0 V at a scan rate of 100 mV s^{-1} for 16 cycles. Then the modified electrode was stabilized for 24 cycles in monomer free 0.5 M H_2SO_4 until a steady state is obtained.

3.4 Oxygen Reduction

The oxygen reduction currents at the different modified electrodes were recorded in oxygen saturated 0.5 M H_2SO_4 solution at a sweep rate of 10 mV s^{-1} between –0.6 V and +0.6 V at various rotational speeds. The reduction currents were normalized to the geometrical area of the electrode (A=0.0707 cm^{-2}).

4 Results and Discussion

4.1 XRD and FTIR characterizations of graphite, GO and rGO.

The XRD result for GO and rGO is shown in Figure 9.

The graphite carbon exhibited two high intensity peaks around 2θ of 24° and 26°and a lower intensity peak at 2θ = 54.7°. However, after chemical oxidation of graphite to GO by the modified Hummer's method, the XRD peaks were shifted to the lower 2θ, indicating that the structure of graphite is changed due to the introduction of oxygen functionalities and water molecule in the structure. GO showed a sharp peak at 2θ =11.38° and a smaller peaks at 2θ of 45° and 80°.

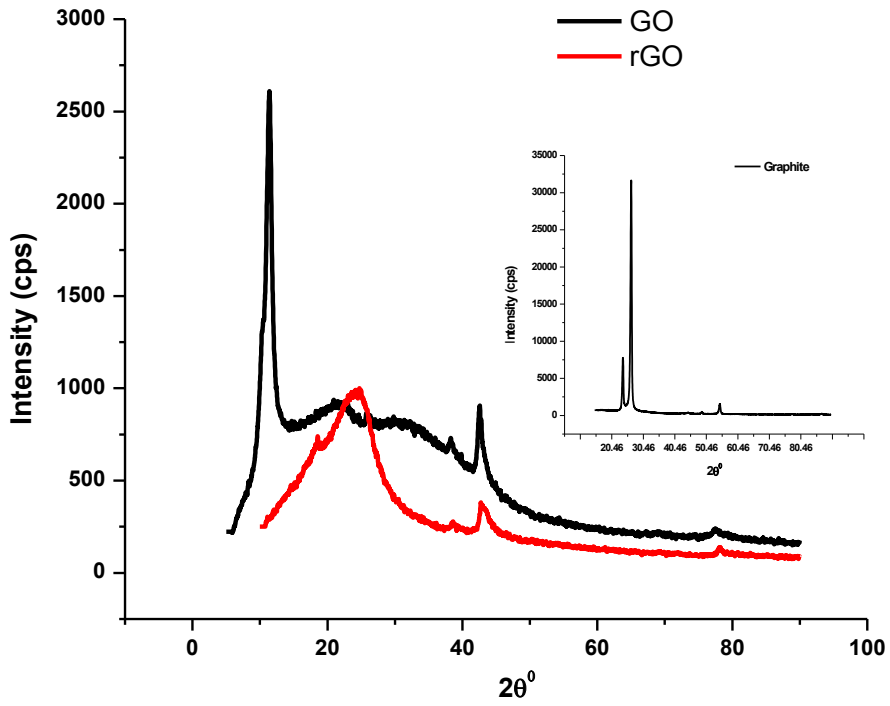

Figure 9. XRD patterns for GO and rGO. Inset: XRD pattern for graphite.

Moreover, rGO revealed that the peaks shifted towards the higher 2θ compared to that of GO. This indicates that the structure of graphene is rearranging after partially reduction of some of

oxygen functionalities in the structure. rGO showed a broad peak centered at 2θ = 24.69º, and, small peaks at 2θ of 45° and 80°.

The FTIR result is shown in Figure 10 and further confirmed the chemical modification of graphite to GO and then to rGO. Upon chemical oxidation of graphite to GO, the characteristic peaks for C=O appear at about 1724 nm and –OH functional groups appear at about 1411 nm and 1219 nm respectively. These peaks disappeared when GO is further chemically reduced to rGO.

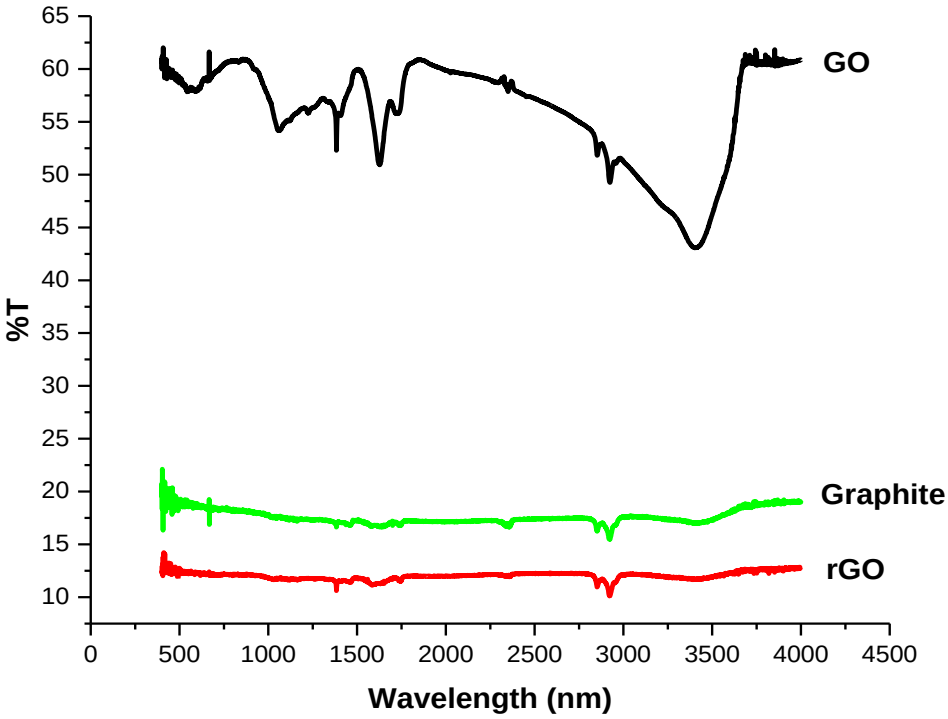

Figure 10. FTIR spectra for graphite, GO and rGO.

4.2 Electrochemical Activities of Graphite, GO and rGO modified GC Electrodes

The electrochemical activities of synthesized GC electrode modified with graphite, GO, and rGO were investigated by recording the cyclic voltammograms using 0.5 mM of $K_3Fe(CN)_6$ mixed in 1.0 M KCl supporting electrolyte. The $K_3Fe(CN)_6$ redox couple was chosen due to its sensitivity to surface chemistry and microstructure [36]. As shown in Figure 11, the oxidation-reduction peak currents of $K_3Fe(CN)_6$ were found to be higher for rGO and graphite modified GC electrode than at bare GC electrode. These peaks were very small at GO modified GCE due to the very low electronic conductivity of GO. Hence, the electrochemical data further supports the changes made during the synthesis of GO and rGO from graphite in agreement with the spectroscopic results.

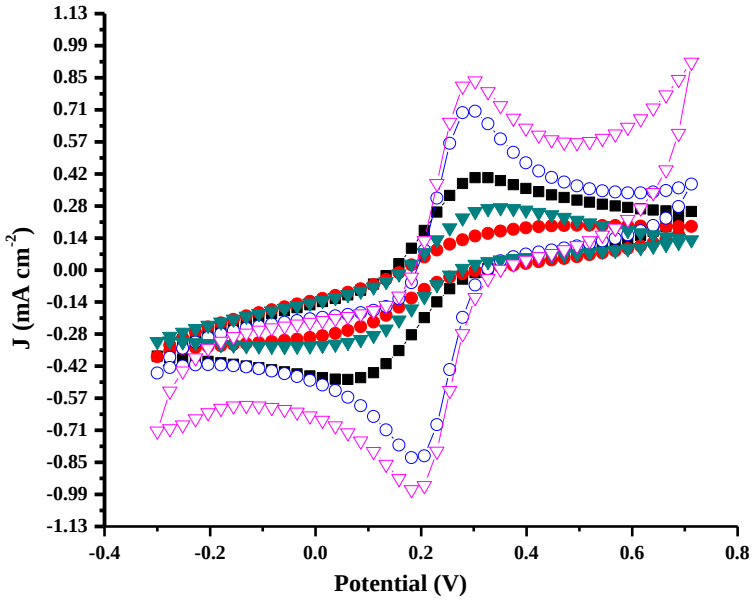

Figure 11. The cyclic voltammograms of samples recorded on bare GC (▼), GO (●), Chemically rGO (○), graphite (■) and electrochemically rGO (∇) modified glassy carbon electrode in 5.0 mM $K_3Fe(CN)_6$ + 1.0 M KCl solution.

4.3 Electrosynthesis of p-(AHNSA) and rGO

After confirming with the synthesis of electronically conductive rGO by electrochemical and spectroscopic methods, p-(AHNSA) were electrodeposited at the rGO modified GCE. Typical CV for the potentiodynamic synthesis was depicted in Figure 12. With increasing the number of cycles an increase in peak currents at about 0.37, 1.69 and –0.14 V were observed. These observations confirm the formation of polymer film at the rGO modified GCE. The number of cycles used in the electropolymerization was 16.

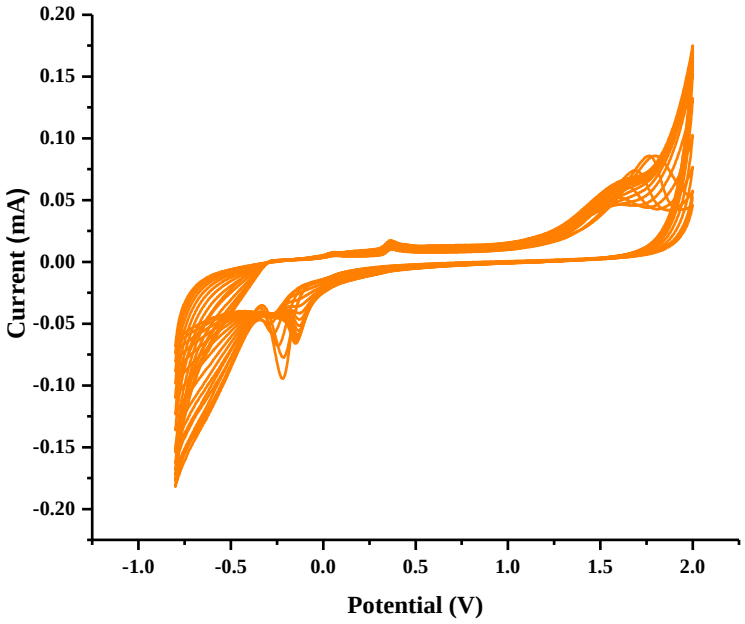

Figure 12. Cyclic voltammograms recorded during the electropolymerization of 2 mM AHNSA in 0.1 M Nitric acid at GCE.

Comparing the CVs of the rGO modified electrode with that of p-(AHNSA) modified rGO/GCE electrode (Figure 13), one observes new redox peaks for the p-(AHNSA) modified rGO/GCE. This also further confirms the electrodeposition of p-(AHNSA) at rGO/GCE.

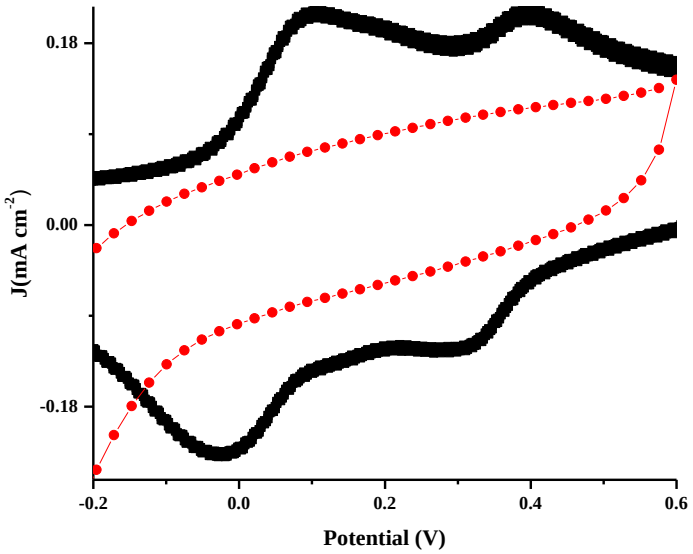

Figure 13. Cyclic voltammograms of rGO/GC (●) and (■) PAHNSA/rGO/GC.

Typical CVs recorded during the electrosynthesis of rGO were depicted in Figure 14. The observed reduction peak for GO in the first scan disappeared in subsequent scans confirming the electrochemical formation rGO.

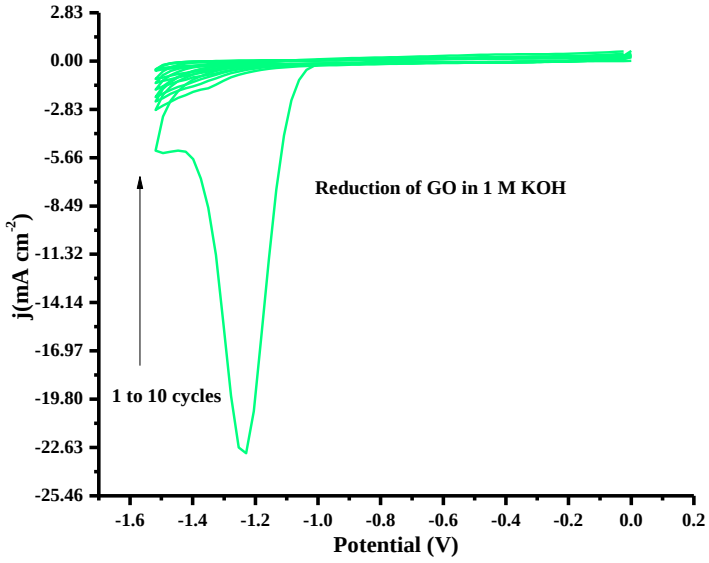

Figure 14. Electrochemical reduction of GO in 1 M KOH solution, for 10 cycles at a scan rate of 50 mV s^{-1}.

4.4 Electrocatalytic reduction of oxygen at modified GCE.

Figure 15 shows typical CVs of N_2 and oxygen saturated 0.5 M H_2SO_4 solution at p-(AHNSA)/rGO/GC at a scan rate of 100 mV s^{-1}. In the CVs of the oxygen saturated 0.5 M H_2SO_4 a new peak started to appear at about -0.32 V which is due to the reduction of oxygen at p-(AHNSA)/ rGO/ modified glassy carbon electrode.

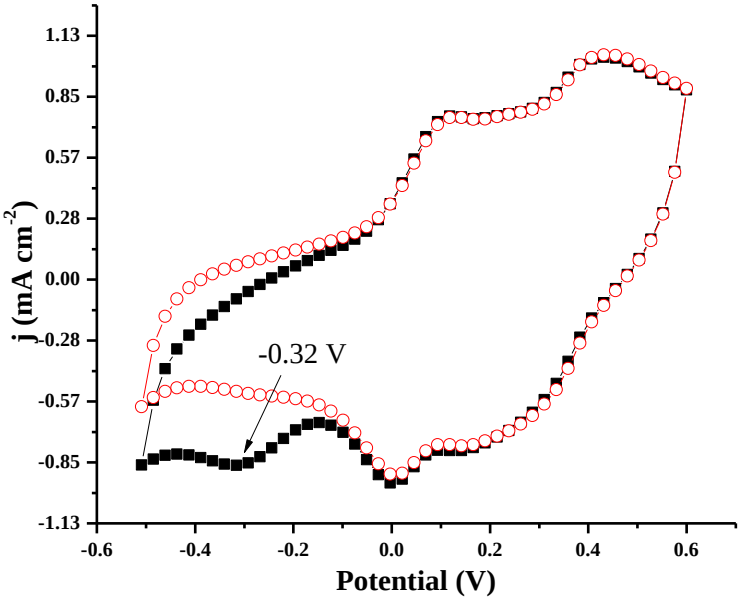

Figure 15. Cyclic voltammograms of O_2 (■) and N_2 (○) saturated 0.5 M H_2SO_4 at p-(AHNSA)/rGO/GCE.

The electrocatalytic activity of p-(AHNSA) modified electrode towards the reduction of oxygen was compared with the other modified electrodes (Figure 16). Electrocatalytic activity for oxygen reduction were not observed for GO and rGO modified GCE. But, the oxygen reduction peak current observed at p-(AHNSA)/GCE were significantly increased at p-(AHNSA)/rGO/GCE. The reduction potential was also shifted anodically. These confirm that the electrocatlytic activity of the p-(AHNSA)/rGO/GCE were better than the p-(AHNSA)/GCE.

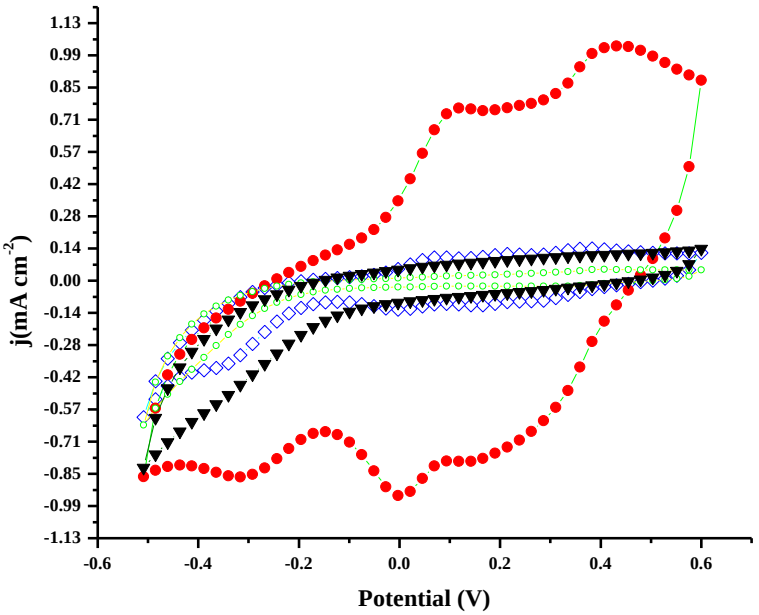

Figure 16. Cyclic voltammograms for the reduction of oxygen, saturated in 0.5 M H_2SO_4 at P-(AHNSA)/rGO/ GC (●), p- AHNSA/GC (◊), rGO/GC (▼), and GO/GC (○).

The linear sweep voltammograms for the reduction of oxygen at p-(AHNSA)/GCE and p-(AHNSA)/rGO/GCE were also recorded at different rotation speeds and depicted in Figure 17 (a) and (b), respectively.

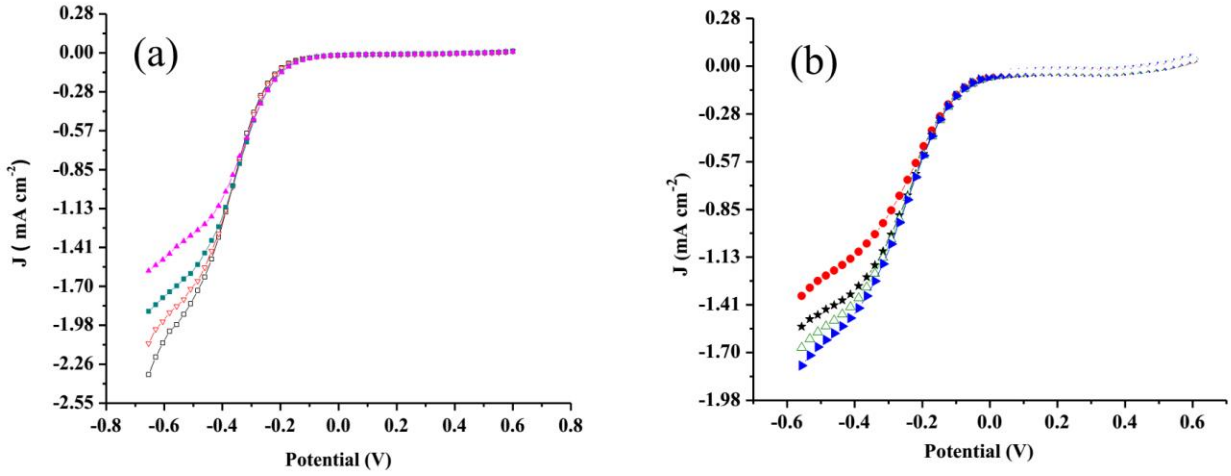

Figure 17. (a) Current vs. potential plot of p-(AHNSA)/GCE at different rotational speed: 1000 rpm (▲),1500 rpm (■), 2000 rpm (∇), 2500 rpm (□) in oxygen saturated 0.5 M H_2SO_4, at scan rate of 10 mV s^{-1}, at 25^0C. And (b) Current vs. potential plot of p-(AHNSA)/rGO/GCE at different rotational speed: 1000 rpm (●),1500 rpm (⋆), 2000 rpm (Δ), 2500 rpm (▼) in oxygen saturated 0.5 M H_2SO_4, at scan rate of 10 mV s^{-1}, at 25^0C.

Figure 17, (a) and (b) are current vs. potential plots for p-(AHNSA)/GCE and p-(AHNSA)/rGO/GCE respectively. Hence, from these plots we obtained Koutecky-Levich plots (i.e. j^{-1} vs. $\omega^{-\frac{1}{2}}$) at different potentials for both p-(AHNSA)/GCE and p-(AHNSA)/rGO/GCE, Figures 19 and 20. From intercept of Figures 19 and 20 we obtained the inverse of kinetic current density (j_k) [38].

The enhanced electrocatalytic activity at p-(AHNSA)/rGO/GCE can be seen by the anodic shift in the oxygen reduction potential in Figure 18.

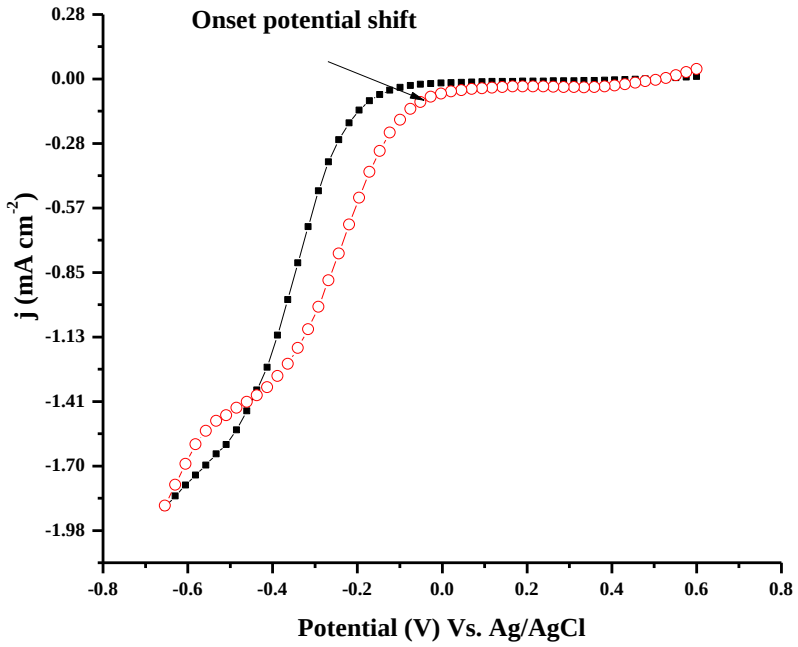

Figure 18. Comparison of the oxygen reduction at p-(AHNSA)/GCRDE (■) and p-(AHNSA)/rGO/GCRDE (○).

Figures 19 and 20 show the K-L plots (j^{-1} vs. $\omega^{-\frac{1}{2}}$) of data taken from Figure 17 (a) and (b) at different electrode potentials.

These K-L plots were used to determine the inverse of kinetic current density and the number of electrons transferred in the reaction, from the intercept and slope respectively [38].

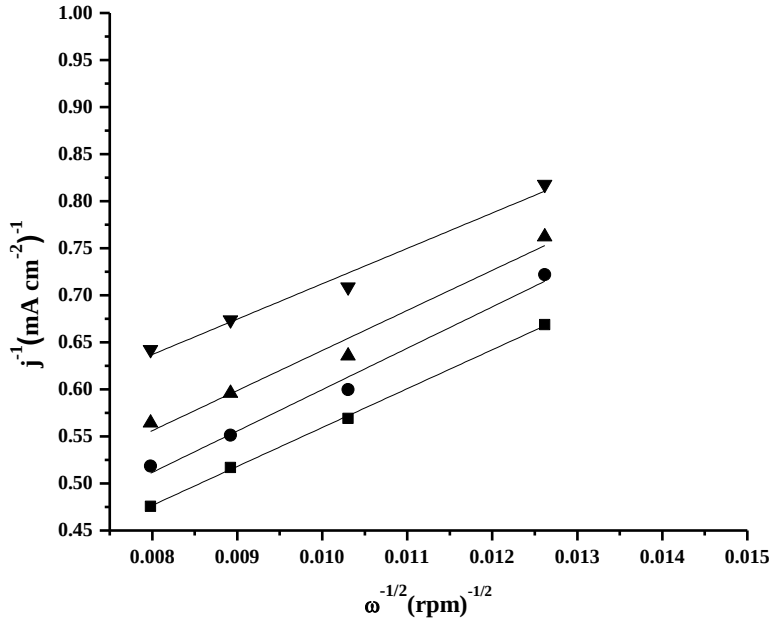

Figure 19. Koutecky-Levich plot for the reduction of oxygen saturated 0.5 M H_2SO_4 at p-AHNSA/GCE at different potentials (-0.45 (▼), -0.50 (▲), -0.55 (●), -0.60 (■). Scan rate: 10 mV s^{-1} and temperature 25^0C.

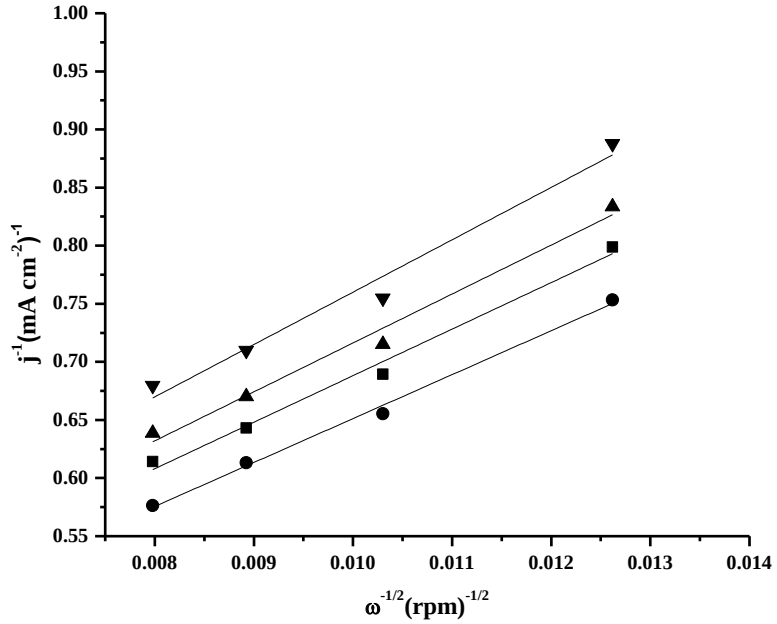

Figure 20. Koutecky-Levich plot for the reduction of oxygen saturated 0.5 M H_2SO_4 at p-AHNSA/rGO/GCE at different potentials (-0.40 (●), -0.45 (■), -0.50 (▲), -0.55 (▼). Scan rate: 10 mV s^{-1} and temperature 25^0C.

The values used for calculatimg number of electrons are: C is the concentration of oxygen in the electrolyte 1.1 mM , D is the diffusion coefficient of O_2 ($2.1x10^{-5}cm^2s^{-1}$) in 0.5 M H_2SO_4, ν is the kinematic viscosity of the electrolyte ($1.075x10^{-2}cm^2s^{-1}$), and ω is the electrode rotational speed (rpm) (from equation 2.6).

Straight lines yielded $n \approx 2$ and $n \approx 4$ over a wide potential range of - 0.40 up to - 0.55 V for p-(AHNSA)/GCE and p-(AHNSA)/rGO/GCE, respectively.

This is done by comparing the slopes of theoretical $4e^-$ and $2e^-$ pathway with the experimental from Koutecky-Levich plots [38].

In Figure 21 and 22, K-L plots of p-(AHNSA)/GCE and p-(AHNSA)/rGO/GCE were plotted and compared with the theoretical two and four electrons K-L plots. A slope very close to two

electron (n=2.50) and four electrons (n=3.70) reduction of oxygen were observed at p-(AHNSA)/GCE and p-(AHNSA)/rGO/GCE. These results further confirm that p-(AHNSA)/rGO/GCE is a better electrocatalyst for oxygen reduction than that of p-(AHNSA)/GCE.

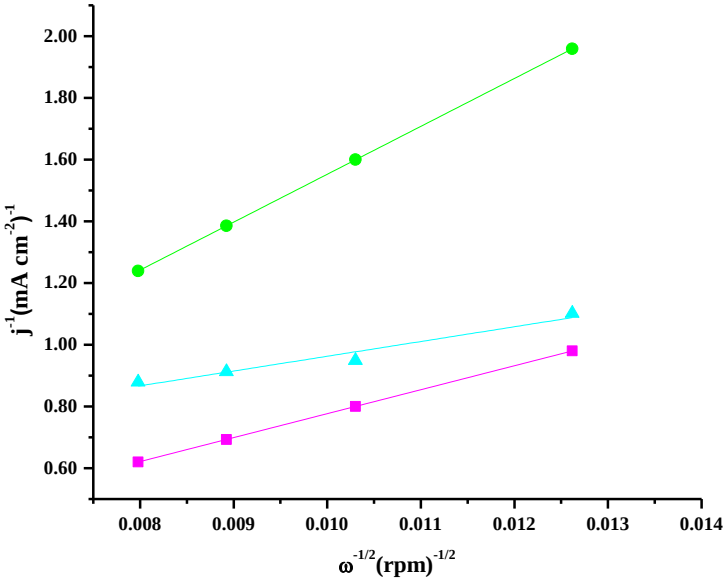

Figure 21. Koutecky-Levich plots for the reduction of oxygen at p-(AHNSA)/rGO modified glassy carbon electrode (O_2 saturated 0.5 M H_2SO_4, 10 mV s^{-1}) including the theoretical for 2e (●) and 4e (■) plus the experimental result (▲).

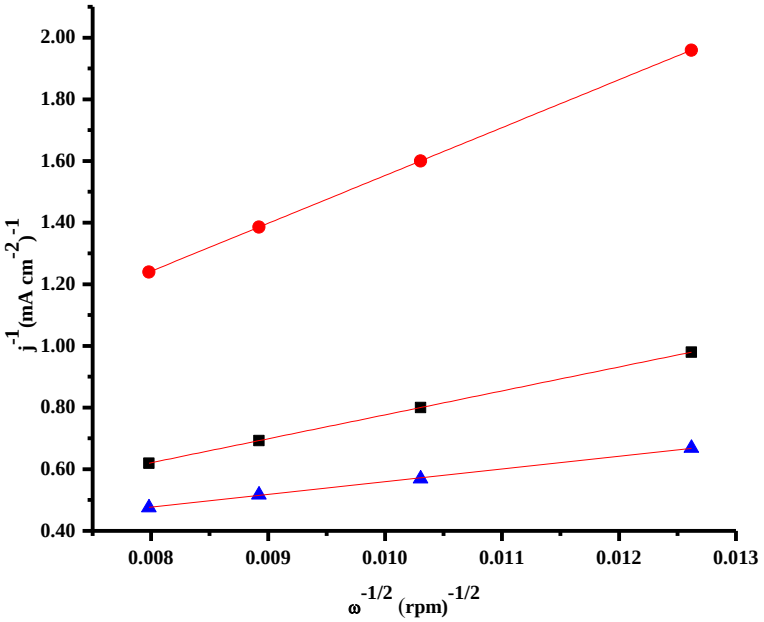

Figure 22. Koutecky-Levich plots for the reduction of oxygen at p-(AHNSA) modified glassy carbon electrode (O_2 saturated 0.5 M H_2SO_4, 10 mV s^{-1}) including the theoretical for 2e (●) and 4e (■) plus the experimental result (▲).

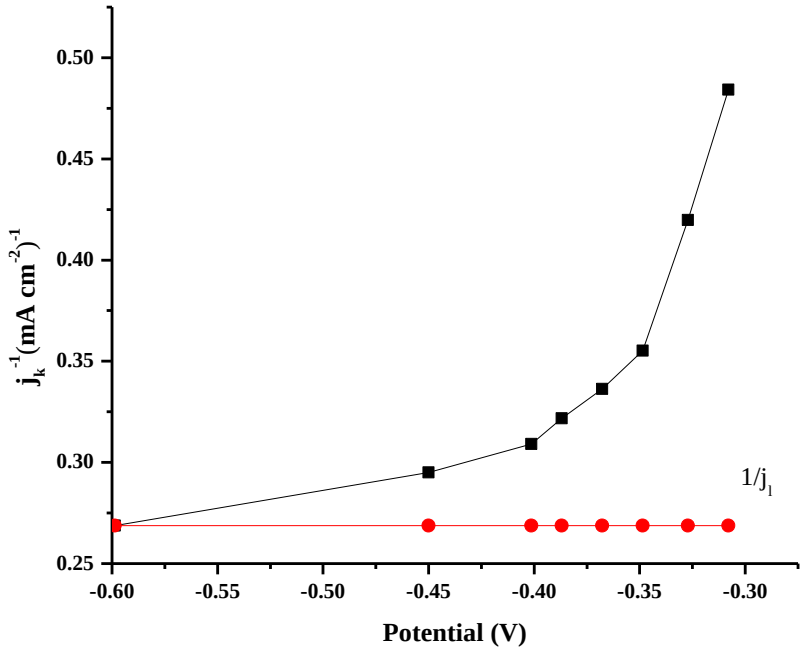

Figure 23. Plot of j_k^{-1} vs. the electrode potential for the reduction of oxygen on p-(AHNSA)/rGO modified glassy carbon rotating disk electrode (in O_2 saturated 0.5 M H_2SO_4).

As can be seen from Figures 23 and 24, for high overvoltage the quantity j_k^{-1} approaches to j_l^{-1} (the limiting current density). (Equation 2.7).

Therefore, the values of the inverse of limiting current densities (j_l^{-1}) were determined from the plots of j_k^{-1} vs. electrode potential (V) for each p-(AHNSA)/GCE and p-(AHNSA)/rGO/GCE.

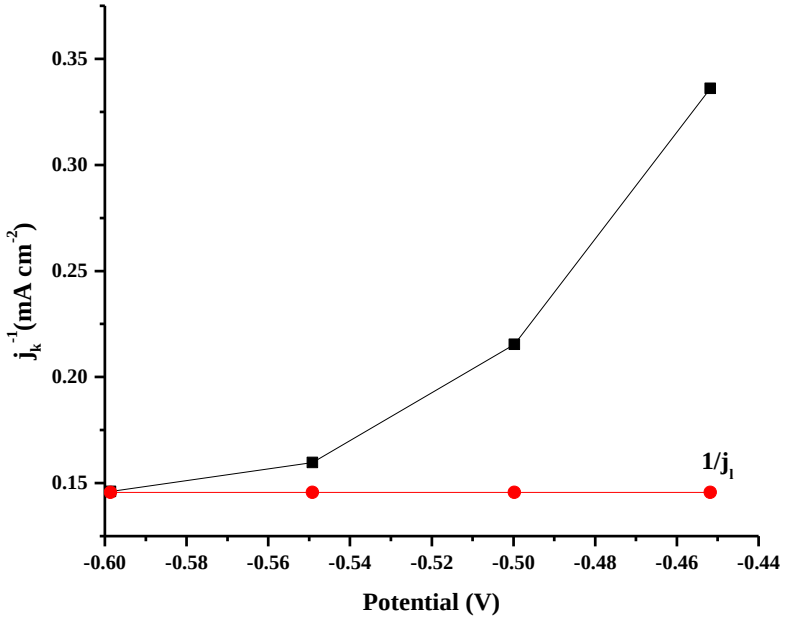

Figure 24. Plot of j_k^{-1} vs. the electrode potential for the reduction of oxygen on p-(AHNSA) modified glassy carbon rotating disk electrode (in O_2 saturated 0.5 M H_2SO_4).

Figure 25 and 26 shows E vs. $\ln[\frac{j_k}{j_l - j_k}]$ p-(AHNSA)/GCE and p-(AHNSA)/rGO/GCE respectively.

These plots were used to determine the exchange current densities (j_0) and the Tafel slopes for each p-(AHNSA)/GCE and p-(AHNSA)/rGO/GCE.

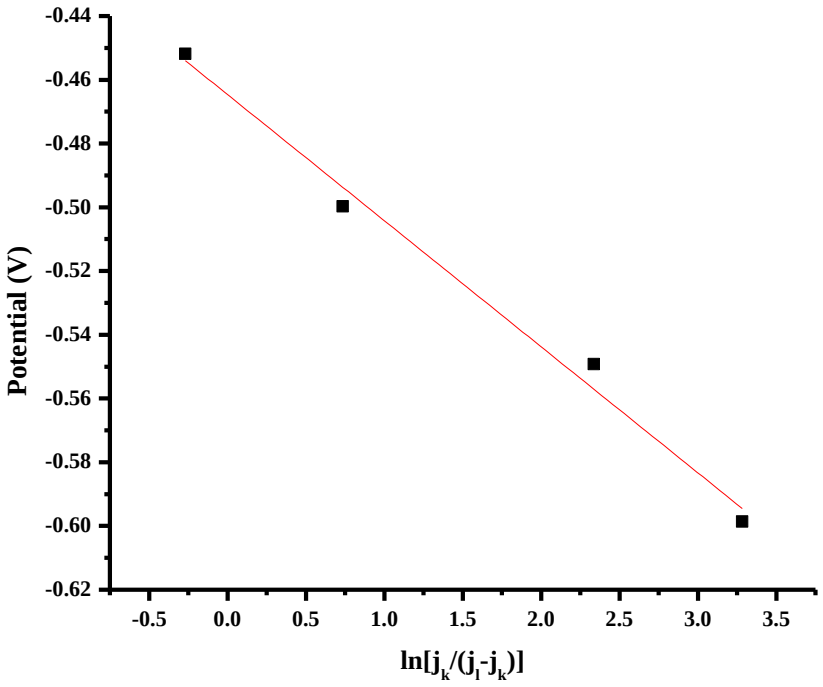

Figure 25. Plot of potential (E) vs. $ln\left[\frac{j_k}{j_l - j_k}\right]$ for the reduction of oxygen in oxygen saturated 0.5 M H_2SO_4; at p-(AHNSA)/ GCE.

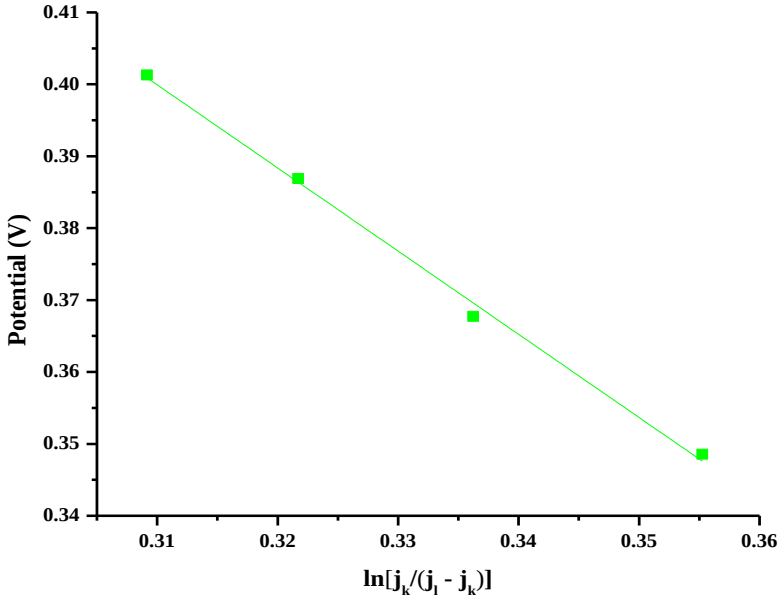

Figure 26. Plot of potential (E) vs. $ln\left[\frac{j_k}{j_l - j_k}\right]$ for the reduction of oxygen in oxygen saturated 0.5 M H_2SO_4; at p-(AHNSA)/rGO/GCE.

The exchange current density j_o and Tafel slope (b) were evaluated from the intercept and slope of the plot; E vs. $\ln[\frac{j_k}{j_l - j_k}]$ in Figure 25 and 26. The results obtained for the exchange current density and limiting current density for p-(AHNSA)/rGO/GCE and p-(AHNSA)/GCE is shown in Table 1 below.

Table 1. Kinetic parameters for oxygen reduction reaction at p-(AHNSA)/rGO/GCE and p-(AHNSA)/GCE.

GC modified with	Limiting current density (A/cm^2)	Tafel slope (b mV/decade)	Exchange current density j_o (mA/cm^2)
p-(AHNSA)	$6.866x10^{-3}$	36.76	$2.156x10^{-5}$
p-(AHNSA)/rGO	$3.72x10^{-3}$	110	$1.88x10^{-3}$

5 Conclusions

The graphene oxide was successfully prepared by oxidizing graphite via the modified Hummer's method. The spectroscopic as well as the electrochemical data confirmed that graphite is oxidized by strong oxidants and the oxygen atoms are introduced into the graphite layers. The data also confirmed that the functional groups in the GO can be further reduced by chemical means forming rGO.

Finally, the electropolymerized p-(AHNSA)/rGO/GCRDE was found to have better electrocatalytic activity towards oxygen reduction reaction compared to p-(AHNSA)/GCRDE. Anodic shift of the onset potential as well as a 4-electron path way were observed for oxygen reduction at p-(AHNSA)/rGO/GCRDE. Kinetic parameters like j_o, j_l, and Tafel slope were evaluated. Good catalytic activity was observed with p-(AHNSA)/rGO/GCE.

6 References

1. S.A. Kumar, S.C., Electrocatalytic Reduction of Oxygen and Hydrogen peroxide at poly (p-aminobenzene Sulfonic acid) modified glassy carbon electrodes. Molecular Catalysis, 2007. **278**: p. 244.
2. P. Manisankar, A.G., Electrocatalytic Reduction of Dioxygen at the surface of Carbon paste electrodes modified with 9, 10-Anthraquinone Derivatives and Dyes. Electroanalysis, 2005. **17**: p. 1051.
3. H. Park, T.K., D. Park, Y. Shim, Bull, Electrocatalytic Reduction of molecular Oxygen at poly(1,8-diaminonaphthalene) and poly(Co(II)-(1,8-diaminonaphthalene)) coated electrodes. Korean Chem. Soc. , 2006. **27**: p. 1763.
4. Scholz, F., Electroanalytical Methods: Guides to Experiments and Application, 1st ed. Springer, Berlin, 2002: p. 29.
5. M. E. Scofield, H.L., S. S. Wong, A Concise Guide to Sustainable PEMFCs: Recent Advances in Improving both Oxygen Reduction Catalysts and Proton Exchange Membranes. Chem. Soc. Rev., 2015. **44**: p. 5836-5860.
6. Yao Nie, L.L.a.Z.W., Recent advancements in Pt and Pt-free catalysts for oxygen reduction reaction. The Royal Society of Chemistry, 2015. **44**: p. 2168-2201.
7. Yuki Saito, T.K., Voltammetry Theory, Types And Applications. Nova publishers N.Y., 2014.
8. Allen J. Bard, L.R.F., Electrochemical Methods Fundamentals and Applications. 2001: p. 94-104.

9. D.R. Dreyer, S.P., C.W. Bielawski, R.S. Ruoff, The chemistry of graphene oxide. Chem. Soc. Rev., 2010: p. 228–240.

10. S. Gilje, S.H., M. Wang, K.L. Wang, R.B. Kaner, A Chemical Route to Graphene for Device Applications. Nano Lett. , 2007. **7**: p. 3394–3398.

11. S. Eigler, A.H., Chemistry with graphene and graphene oxide - Challenges for synthetic chemists. Angew. Chemie - Int. Ed. , 2014. **53**: p. 7720–7738.

12. S. Pei, H.M.C., The reduction of graphene oxide. Carbon N. Y. , 2012. **50** p. 3210–3228.

13. R. Rozada, J.I.P., S. Villar-Rodil, A. Martnez-Alonso, J.M.D. Tascn, Towards full repair of defects in reduced graphene oxide films by two-step graphitization. Nano Res. , 2013. **6**: p. 216–233.

14. G. Eda, M.C., Chemically Derived Graphene Oxide : Towards Large-Area Thin-Film Electronics and Optoelectronics. Adv. Mater, 2010: p. 2392–2415.

15. G. Eda, G.F., M. Chhowalla, Large-area ultrathin films of reduced graphene oxide as a transparent and flexible electronic material. Nature, Nanotechnol, 2007. **3**: p. 270–274.

16. B.S. Pang, H.N.T., X. Feng, K. Mu, Patterned Graphene Electrodes from Solution-Processed Graphite Oxide Films for Organic Field-Effect Transistors. Adv. Mater, 2009: p. 3488–3491.

17. M.D. Stoller, S.P., Y. Zhu, J. An, R.S. Ruoff, Graphene-based ultracapacitors. Nano Lett., 2008. **8**: p. 3498–502.

18. N.I. Kovtyukhova, P.J.O., B.R. Martin, T.E. Mallouk, S.A. Chizhik, E.V. Buzaneva, and A.D. Gorchinskiy, Layer-by-Layer Assembly of Ultrathin Composite Films from Micron-Sized Graphite Oxide Sheets and Polycations. Chemistry of Materials, 1999. **11(3)**: p. 771-778.

19. Offeman, W.S.H.a.R.E., Preparation of Graphitic Oxide. Journal of the American Chemical Society, 1958. **80(6)**: p. 1339.

20. D.C. Marcano, D.V.K., J.M. Berlin, A. Sinitskii, Z. Sun, A. Slesarev, L.B. Alemany, W. Lu, and J.M. Tour, Improved Synthesis of Graphene Oxide. ACS Nano, 2010. **4(8)**: p. 4806-4814.

21. P. V. Lakshminarayanan, H.T., C.U. Pittman, Nitric acid oxidation of vapor grown carbon nanofibers. Carbon N. Y. , 2004. **42**: p. 2433–2442.

22. N. Zhang, L.W., H. Liu, Q. Cai, Nitric acid oxidation on carbon dispersion and suspension stability. Surf. Iand Nterface Anal, 2008: p. 1190–1194.

23. A. Simon, R.D., B. Krebs, B. Hettich, The Crystal Structure of Mn_2O_7. Angew. Chemie Int. Ed. English, 1987. **26**: p. 139–140.

24. Y. Huang, D.R.P., Effect of MolecularWeight and Temperature on Physical Aging of Thin Glassy Poly(2,6-dimethyl-1,4-phenylene oxide) Films. J. Polym. Sci. Part B Polym. Phys., 2007. **45**: p. 1390–1398.

25. S. Stankovich, D.A.D., R.D. Piner, K.A. Kohlhaas, A. Kleinhammes, Y. Jia, Y. Wu, S.B.T. Nguyen, R.S. Ruoff, Synthesis of graphene-based nanosheets via chemical reduction of exfoliated graphite oxide. Carbon N.Y., 2007. **45**: p. 1558-1565.

26. S. Stankovich, D.A.D., G.H.B. Dommett, K.M. Kohlhaas, E.J. Zimney, E.A. Stach, R.D. Piner, S.T. Nguyen, R.S. Ruoff, Graphene-based composite materials. Nature, 2006. **442**: p. 282–286.

27. H.J. Shin, K.K.K., A. Benayad, S.M. Yoon, H.K. Park, I.S. Jung, M.H. Jin, H.K. Jeong, J.M. Kim, J.Y. Choi, Y.H. Lee, Efficient reduction of graphite oxide by sodium

borohydride and its effect on electrical conductance. Adv. Funct. Mater, 2009. **19**: p. 1987-1992.

28. S.J. Kang, C.K., T. Ozel, M. Shim, N. Pimparkar, M. a Alam, S. V Rotkin, J. a Rogers, High-performance electronics using dense, perfectly aligned arrays of single-walled carbon nanotubes. Nat. Nanotechnol, 2007. **2**: p. 230–236.
29. H.C. Schniepp, J.L.L., M.J. McAllister, H. Sai, M. Herrera-Alonson, D.H. Adamson, R.K. Prud'homme, R. Car, D.A. Seville, I.A. Aksay, Functionalized single graphene sheets derived from splitting graphite oxide. J. Phys. Chem., 2006. **B. 110**: p. 8535–8539.
30. M. Zhou, Y.W., Y. Zhai, J. Zhai, W. Ren, F. Wang, S. Dong, Controlled synthesis of large-area and patterned electrochemically reduced graphene oxide films. Chem. - A Eur. J, 2009. **15**: p. 6116–6120.
31. H.C. Schniepp, J.L.L., M.J. McAllister, H. Sai, M. Herrera-Alonson, D.H. Adamson, R.K. Prud'homme, R. Car, D.A. Seville, I.A. Aksay, Functionalized single graphene sheets derived from splitting graphite oxide. J. Phys. Chem., 2006. **B. 110** p. 8535–8539.
32. S. Gilje, S.H., M. Wang, K.L. Wang, R.B. Kaner, A Chemical Route to Graphene for Device Applications. Nano Lett., 2007. **7**: p. 3394–3398.
33. J.T. Robinson, M.Z., E.S. Snow, J.W. Baldwin, Z. Wei, P. Sheehan, B.H. Houston, Wafer-scale reduced graphene oxide films for nanomechanical devices. Nano Lett., 2008. **8**: p. 3441–5.
34. M. Zhou, Y.W., Y. Zhai, J. Zhai, W. Ren, F. Wang, S. Dong, Controlled synthesis of large-area and patterned electrochemically reduced graphene oxide films. Chem. - A Eur. J. , 2009. **15**: p. 6116–6120.

35. C.Y. Su, A.Y.L., Y. Xu, F.R. Chen, A.N. Khlobystov, L.J. Li, High-quality thin graphene films from fast electrochemical exfoliation. ACS Nano, 2011. **5**: p. 2332–2339.

36. Protti, P., Introduction to Modern Voltammetric and Polarographic Analisys Techniques, Fourth Edition. 2001.

37. Christopher M.A. Brett, A.M.O.B., Electrochemistry Principles, Methods, and Applications. 1994: p. 174-194.

38. Berhanu W. Zewde, S.A., Electrocatalysis of Oxygen reduction at poly(4-amino-3-hydroxynaphthalene sulfonic acid) and platinum loaded polymer modified glassy carbon electrodes. power sources, 2012. **216**: p. 502-507.

39. Yoshio Waseda, E.M., Kozo Shinoda, X-Ray Diffraction Crystallography Introduction, Examples and Solved Problems. 2011.

40. Cullity, B.D., Elements of X-ray Diffraction. 1956.

41. Maas, J.H.v.d., Basic Infrared Spectroscopy Second Edition. 1972.

42. Stuart, B., Infrared Spectroscopy Fundamentals And Applications. 2004.

43. Jingning Shan, P.G.P., Characterization of polymer supported catalysts by cyclic voltammetry and rotating disk voltammetry. Electrochemica Acta, 2000. **46**: p. 119-125.